First-principles study of the origin and nature of ferromagnetism in $Ga_{1-x}Mn_xAs$

Stefano Sanvito*
Materials Department, University of California, Santa Barbara, California 93106

Pablo Ordejón
Institut de Ciència de Materials de Barcelona (CSIC) Campus de la U.A.B, E-08193 Bellaterra, Barcelona, Spain

Nicola A. Hill
Materials Department, University of California, Santa Barbara, California 93106
(Received 3 November 2000; published 4 April 2001)

The properties of diluted $Ga_{1-x}Mn_xAs$ are calculated for a wide range of Mn concentrations within the local-spin-density approximation of density-functional theory. Mülliken population analyses and orbital-resolved densities of states show that the configuration of Mn in GaAs is compatible with either $3d^5$ or $3d^6$; however, the occupation is not integer due to the large *p-d* hybridization between the Mn *d* states and the valence band of GaAs. The spin splitting of the conduction band of GaAs has a mean-field-like linear variation with the Mn concentration, and indicates ferromagnetic coupling with the Mn ions. In contrast, the valence band is antiferromagnetically coupled with the Mn impurities, and the spin splitting is not linearly dependent on the Mn concentration. This suggests that the mean-field approximation breaks down in the case of Mn-doped GaAs, and corrections due to multiple scattering must be considered. We calculate these corrections within a simple free-electron model, and find good agreement with our *ab initio* results if a large exchange constant ($N\beta = -4.5$ eV) is assumed.

DOI: 10.1103/PhysRevB.63.165206 PACS number(s): 75.50.Pp, 75.30.Et, 71.15.Mb, 71.15.Ap

I. INTRODUCTION

The discovery of ferromagnetic order in diluted magnetic semiconductors (DMS's) made of heavily Mn-doped InAs (Ref. 1) and GaAs (Refs. 2–4) paved the way for many semiconductor spin devices.[5] In particular the ferromagnetism of $Ga_{1-x}Mn_xAs$ adds the spin degree of freedom to the GaAs/(Al, Ga)As system which, in the last few years, has been the benchmark for interesting physics and for high-speed electronic and optoelectronic devices.

The long spin lifetime[6] and spin coherence[7] of GaAs have already been demonstrated. Recently the feasibility of spin injection into GaAs using $Ga_{1-x}Mn_xAs$ contacts was proved[8] overcoming the intrinsic difficulty of injecting spins into semiconductors from magnetic metals.[9] These two effects suggest that the GaAs/(Al, Ga)As/$Ga_{1-x}Mn_xAs$ system is the best candidate for injecting, storing, and manipulating spins in entirely solid-state devices; a valuable step toward a practical realization of quantum computing.[10]

Although there is general agreement on the carrier-(hole-) mediated origin of the ferromagnetism in $Ga_{1-x}Mn_xAs$, the detailed mechanism is still a matter of debate.[11–13] Recently Dietl *et al.* studied the ferromagnetism of III-V DMS's within the Zener model, and obtained good agreement with existing experimental data using a few phenomenological parameters. One of the key elements of the model is the mean-field Kondo-like coupling (*p-d* Hamiltonian) between the valence band of the host semiconductor and the magnetic impurity,

$$H_{\text{sp-}d} = -N\beta \vec{s}\cdot\vec{S}, \tag{1}$$

where $N\beta$ is the *p-d* exchange constant, $\vec{s}$ is the valence-band electron spin, and $\vec{S}$ is the impurity spin. In this model the exchange constant, which governs the spin splitting of the valence band of the host semiconductor, enters quadratically into the expression for the Curie temperature. Therefore, its exact evaluation is crucial for making quantitative predictions about the ferromagnetism in both existing and possibly new materials.

Unfortunately, in contrast with the case of II-VI DMS's, the experimental determination of $N\beta$ is not conclusive, and both the sign and the magnitude are not well known, particularly for large Mn concentrations ($x > 0.01$). From the exciton splitting in the low dilution limit ($x < 0.001$) the coupling is found to be ferromagnetic, with an exchange constant of $N\beta = +2.5$ eV,[14] if the exchange constant for the conduction band $N\alpha$ is assumed to be $+0.2$ eV (a typical value for Mn in II-VI semiconductors). Reflectance magnetic circular dichroism[15] and magnetoabsorption experiments[16] present controversial results, since the absorption edge splitting is strongly dependent on the hole concentration (the Moss-Burstein effect), which in turn is difficult to determine from transport measurements because of a strong magnetoresistance up to very high magnetic fields.[3] Magnetotransport experiments are able to measure only the magnitude of the exchange constant, and the values obtained vary from $|N\beta| = 3.3$ eV (Ref. 17) to $|N\beta| = 1.5$ eV.[18] Finally a recent core-level photoemission study[19] of $Ga_{0.926}Mn_{0.074}As$ gave $N\beta = -1.2$ eV if a Mn^{2+} configuration is assumed. Nevertheless it is worth noting that the raw data are compatible with both the Mn^{2+} and Mn^{3+} configurations, and so one cannot make a definite determination of the sign of $N\beta$.

From a theoretical point of view, the exchange interaction for the conduction band results from a direct Coulombic ex-

change, and is expected to be ferromagnetic. In contrast, the exchange interaction of the valence band has a kinetic-energy origin,[20] and the sign and strength of the coupling depend critically on the population of the spin-polarized Mn *d* shell. Three types of Mn centers in GaAs are possible. The first two can be seen as substitutional Mn^{3+} and Mn^{2+}, respectively, with the former neutral (A^0 with formal $3d^4$ configuration) with spin $S=2$ and the latter negatively charged (A^- with formal configuration $3d^5$) with spin $S=\frac{5}{2}$. The third center is obtained when A^- weakly binds a hole, forming a neutral $(3d^5+h)$ complex. The A^- center provides only antiferromagnetic coupling with the valence band, while the neutral A^0 centers can provide either ferromagnetic or antiferromagnetic[21] coupling.

From this brief overview it is clear that a detailed description of the electronic structure of Mn in GaAs is crucial to understand and correctly model the ferromagnetism of $Ga_{1-x}Mn_xAs$. In this paper we address this issue by calculating the ground-state properties of $Ga_{1-x}Mn_xAs$ over a range of Mn concentrations using density functional theory (DFT)[22] in the local-spin-density approximation (LSDA). We use a numerical implementation of DFT based on pseudopotentials and pseudoatomic orbitals.[23–25] Although the convergence versus basis set with localized orbitals is more difficult than with plane waves (where a single parameter, the energy cutoff, determines the completeness of the basis), the method has the great advantage of being able to handle a large number of atoms with an accuracy comparable to plane-wave methods. This allows us to investigate various Mn dilutions without the need of large computer resources. Moreover the pseudoatomic basis is very convenient for analysis of atomic occupation and orbital-resolved densities of states (DOS's), since no overlap integrals between different bases have to be calculated.

The remainder of this paper is organized as follows. In Sec. II we provide some technical details about the calculation method, illustrating in particular how to optimize the pseudoatomic basis set. Then we present our results for $Ga_{1-x}Mn_xAs$ for Mn concentrations ranging from $x=1$ to 0.02. We analyze the density of states projected onto the different orbital components and the charge distribution around the Mn ions, and we perform Mülliken population analyses to determine the occupation of the *d* orbitals of Mn. In Sec. IV we discuss the *p-d* exchange constant and compare our results with that expected from the Kondo-like effective Hamiltonian [Eq. (1)] in the mean-field approximation. Then we illustrate how the mean-field picture breaks down in the case of Mn in GaAs and how the local-density-approximation (LDA) results can be explained by a simple model which includes multiple scattering contributions. Finally in Sec. VI we present our conclusions.

II. COMPUTATIONAL TECHNIQUE

Since we are interested in a calculation of the electronic properties of diluted alloy systems, we need a method that is able to handle a large number of atoms with sufficient accuracy within a periodic supercell approach. For this purpose, we use a DFT approach based on pseudopotentials, and numerical localized atomic orbitals as basis sets. This method, implemented in the code SIESTA,[23–25] combines accuracy and a small computational cost compared to other approaches with considerably larger computational requirements, such as plane waves. In this approach, however, special care must be devoted to an optimization of the basis set, in order to obtain the desired accuracy. In this section, we describe the optimization procedure used in this work. For all the DFT calculations presented here, we use the Ceperley-Alder[26] form of the exchange-correlation potential. Self-consistency is achieved using the Pulay density mixing scheme,[27] with a convergence criterion of 10^{-6} for the change in the elements of the density matrix.

A. Pseudopotentials

We use the widely used scalar relativistic Troullier-Martins pseudopotentials[28] with nonlinear core corrections[29] and Kleinman-Bylander factorization.[30] The reference configurations are $4s^24p^03d^5$, $4s^24p^33d^0$ and $4s^24p^13d^0$, respectively, for Mn, As, and Ga. The cutoff radii for the *s*, *p*, and *d* components of the pseudopotential are (1) 2.00, 2.20 and 1.90 a.u. for Mn; (2) 1.90, 2.20, and 2.50 a.u. for As; and (3) 2.10, 2.50, and 3.0 a.u. for Ga. We check the pseudopotentials at the atomic level by comparing the pseudoeigenvalues with those generated by all electron calculations for several atomic and ionic configurations.

In order to check the transferability of the pseudopotentials just described, we have chosen to use a plane-wave method.[31] This allows us to perform essentially converged calculations with respect to the basis set (by using a sufficiently large energy cutoff for the plane waves), and to isolate pseudopotential effects from basis set effects in checking the pseudopotential. We have computed the equilibrium lattice constant and the band structures of both GaAs and MnAs, both of them showing good agreement with previously published results.[32]

After testing the pseudopotential, we have also calculated the band structure for a fixed localized orbitals basis set over a range of pseudopotential cutoff radii. Our results show as expected, that pseudopotentials that yield the best results with plane waves also give the best band structures with the localized atomic orbitals.

B. Basis set: Number of ζ's

Let us now turn our attention to the pseudoatomic basis set. The procedure to generate the numerical atomic orbitals was described in Ref. 33. The atomic orbitals are constructed as the product of an angular function with a given angular momentum *l* (yielding to *s*-type, p_x, p_y, p_z-type, etc. orbitals), and a numerical radial function. Several functions with the same angular and different radial form can be considered to represent the same atomic shell, referred to as multiple-ζ functions. The radial functions are determined as follows: the first ζ's are obtained, according to the scheme proposed by Sankey and Niklewsi,[34] as confined pseudoatomic orbitals (PAO's) which result from the DFT solution of the free atom with the pseudopotential and a spherical potential of radius r_c. The pseudo-wave-function $\phi(r)$ constructed in such a

way extends only to distances smaller than the cutoff radius r_c. Note that this does not correspond to a simple truncation, since the pseudo-wave-function is continuous at $r=r_c$. Second and successive ζ's are constructed in a split-valence spirit. They are obtained by subtracting from the first ζ a function which reproduces the tail of the pseudoatomic orbital for $r>r_{DZ}$ and continues toward the origin as $r^l(a-br^2)$. Here l is the angular momentum, a and b are parameters chosen to ensure the continuity, and DZ refers to ''double-ζ.'' r_{DZ} is chosen in such a way that the total norm beyond this radius has a certain value. In the present calculation we always fix the norm beyond r_{DZ} to 15% of the total norm, noting that small variations around that value do not produce any significant changes in the total energy. Further ζ's are calculated by repeating the same scheme. This approach is more efficient than using excited states of the neutral atom, which can be unbound.[33]

The optimization of the PAO basis is more delicate than that of its plane-wave counterpart. In the case of the PAO bases used here, several parameters determine the accuracy of the basis: the number of ζ's for each shell, the angular momentum components included, the confinement radii, etc. All these must be optimized to achieve the required accuracy. Since we are interested in describing the magnetic properties of $Ga_{1-x}Mn_xAs$, it is natural to choose a magnetic quantity as the one to monitor the convergence of our results with respect to the basis set quality. We study the energy difference Δ_{FA} between the antiferromagnetic and ferromagnetic alignments of two Mn atoms in a four-atom unit cell of zinc-blende MnAs as a function of the basis set. The lattice constant is chosen to be $a_0=5.8$ Å, which is the critical lattice constant for the half-metallic behavior of MnAs.[32]

The first problem we address is the number of ζ's to include for each atomic orbital. We start by choosing double-ζ for the s orbitals of both Mn and As, and single-ζ for the p and d orbitals of Mn; then we progressively increase the number of basis orbitals. The initial cutoff radii are $r_c=6.0$ a.u. for the s and p orbitals of Mn, $r_c=5.0$ a.u. for the d orbital of Mn, and $r_c=5.5$ a.u. for the s and p orbital of As. These are proportional to the positions of the maxima of the unconstrained pseudo-wave-functions.

In Fig. 1 we present the total energies for the ferromagnetic (E_{FM}) and antiferromagnetic (E_{AF}) alignments, and Δ_{FA}, for the different PAO bases listed in Table I. From the picture two important conclusions can be reached. First, according to the usual variational principle, the total energies for both ferromagnetic and antiferromagnetic configurations decrease with an enlargement of the basis. Second, the split between the ferromagnetic and antiferromagnetic configurations is significantly reduced by using triple-ζ's for the d orbitals of Mn (note the large decrease of Δ_{FA} when going from basis 1 to basis 2 and from basis 4 to basis 5) and double-ζ for the p orbitals of As. This sensitivity of the magnetic phase stability to the As-p and Mn-d basis is consistent with the magnetism in MnAs being driven by strong p-d hybridization. Since we are mainly interested in the magnetic properties of diluted systems describable by very large unit cells, we decide to use double-ζ for all the orbitals except the

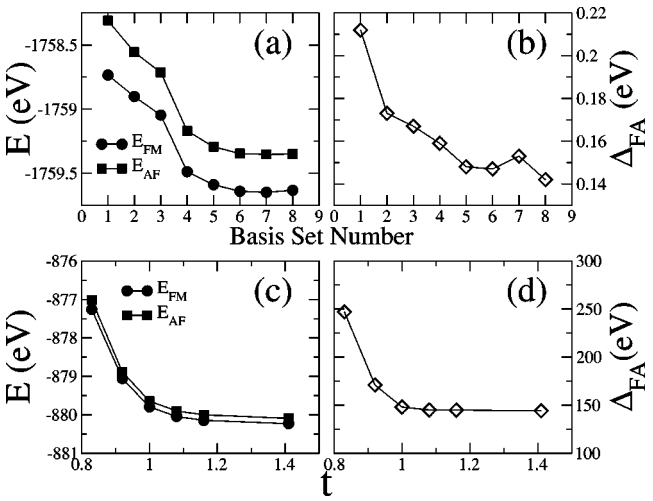

FIG. 1. (a) E_{FM}, E_{AF}, and (b) Δ_{FA} for the basis of Table I. Note the decrease of the total energies as the basis becomes more complete. Δ_{FA} saturates for basis 5. In (c) and (d), respectively, E_{FM}, E_{AF}, and Δ_{FA} stand for the fifth basis set of table I as a function of the scaling parameter t. Note that Δ_{FA} saturates sooner than the total energies for ferromagnetic and antiferromagnetic alignments.

d orbitals of Mn for which we use triple-ζ (this is the fifth basis set in Table I). Note that we can afford to use triple-ζ for Mn-d, since few Mn ions are present in the cell. In contrast, the use of larger basis sets for Ga and As yields a more dramatic increase of the size of the computations.

C. Basis set: Cutoff radii

Next we turn our attention to the choice of the cutoff radii of the basis sets. For free atoms, the optimum cutoff radius of any orbital (as the one which minimizes the energy) is infinite, since that case corresponds to no confinement potential, which yields to exponential tails for all the atomic wave functions. However, in solids this criterion does not hold, since the lack of vacuum and the presence of a crystal potential tend to confine the atomic wave functions more than in the free atom. In this situation, the confinement of each PAO should be optimized to minimize the total energy. This procedure has shown in other systems, such as bulk bcc Fe,[35] that a finite and relatively small confinement radius can pro-

TABLE I. Summary of the bases used in Fig. 1. In the first column we show the indicator of the basis, and the following columns show the number of ζ (N_ζ) for each orbital.

Basis	N_ζ (As s)	N_ζ (As p)	N_ζ (Mn s)	N_ζ (Mn p)	N_ζ (Mn d)
1	2	1	2	1	1
2	2	1	2	1	2
3	2	1	2	2	2
4	2	2	2	2	2
5	2	2	2	2	3
6	2	2	3	2	3
7	2	3	2	2	3
8	2	2	2	3	3

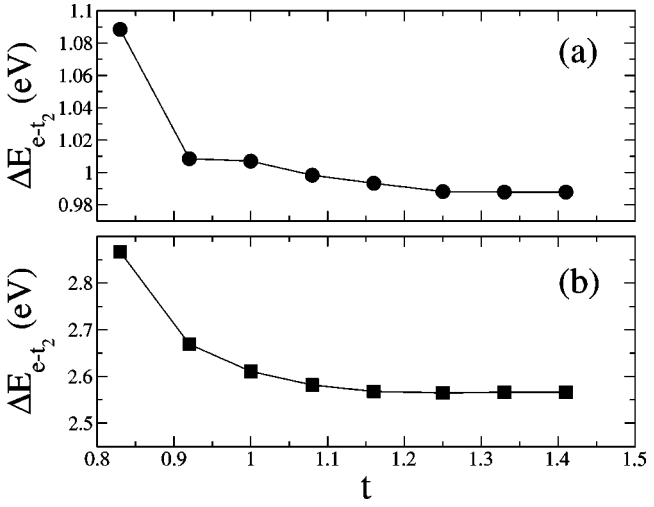

FIG. 2. e-t_2 energy split at the Γ point for MnAs: (a) majority spin, (b) minority spin.

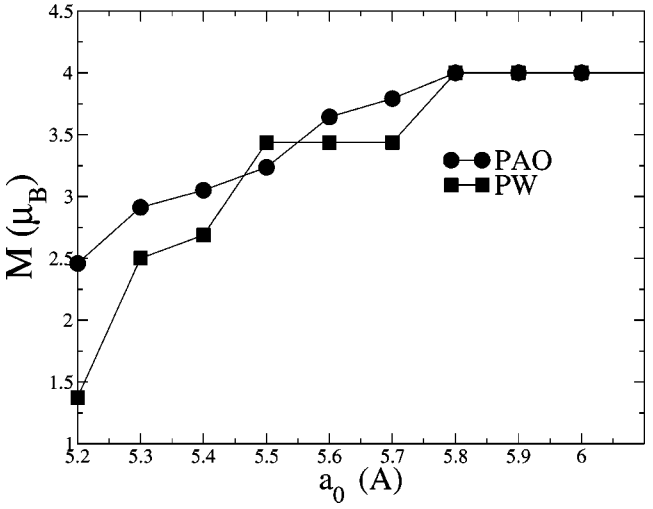

FIG. 3. Magnetization as a function of the lattice constant for zinc-blende MnAs.

vide lower energies and therefore more accurate bases than long values of r_c. These calculations also show that the optimum confinement radius of each PAO depends very much on the particular orbital. In our case, however, it would be too complex to optimize r_c for all the orbitals in our system, due to the large number of these. Instead, we have followed a simpler approach. We vary the initial cutoff radii uniformly by multiplying all the radii by a common scaling factor t. A somewhat similar criterion is to use the orbital energy shift ΔE_{PAO} as the variational parameter, which is the energy increase that each orbital experiences when confined to a finite sphere, and can be used as single parameter to test the convergence.[33]

In Figs. 1(c) and 1(d) we present E_{FM}, E_{AF}, and Δ_{FA} as functions of t for the fifth basis set of Table I. The last point in Figs. 1(c) and 1(d) ($t=1.41$) corresponds to a basis with an orbital energy shift ΔE_{PAO} of 0.001 Ry. A convergence of 0.001 Ry was successfully used to describe the magnetic properties of Ni clusters on Ag surfaces,[36] and is considered an optimal value for the convergence. However, in our case we prefer to use smaller cutoff radii in order to reduce the computation time. From Fig. 1(d) it is clear that the saturation of Δ_{FA} occurs for shorter radii than those required to converge the total energies. We therefore decide to fix the cutoff radii to $t=1$, noting that E_{FM} and E_{AF} differ from the value obtained for $\Delta E_{\mathrm{PAO}}=0.001$ Ry by only 0.04%, and that Δ_{FA} differs by only 2%.

D. Comparison with previous calculations

We further test our basis set by computing the energy split between Mn d states with e and t_2 symmetry at the Γ point, and the dependence of the magnetization on the lattice spacing for zinc-blende MnAs. These two tests give an indication of the accuracy of the p-d exchange, which is a dominant interaction in $Ga_{1-x}Mn_xAs$. In fact, at the Γ point the t_2 states are coupled with the As-p states, while the e states are decoupled, and their splitting is determined by the p-d coupling.

In Fig. 2 we present the energy split $\Delta E_{e\text{-}t_2}=E_e-E_{t_2}$ as a function of t for both the spin directions. The e-t_2 split converges monotonically, and there is a variation of only $\sim$2% going from $t=1$ to 1.41 ($\Delta E_{\mathrm{PAO}}=0.001$ Ry). If we now compare this result with our previously published results[32] obtained with plane waves, we note that our present results give an e-t_2 splitting around 50 meV less than the plane-wave splitting for both spins. This is roughly the same dis-

TABLE II. Kohn-Sham eigenvalues calculated using various methods. The energies are calculated with respect to the top of the valence band, and all the units are eV. $\mathrm{PAO_{expt}}$ and $\mathrm{PAO_{theor}}$ are the results of the present calculation assuming the lattice constant to be the experimental value $a_0=5.65$ Å and the theoretical value $a_0=5.635$ Å, respectively. LAPW stands for linear augmented plane wave and PW-PP for plane wave pseudopotentials.

GaAs	Γ_1	Γ_1	X_1	X_3	X_5	X_1	L_2	L_1	L_3	L_1
$\mathrm{PAO_{expt}}$	−12.91	0.57	−10.53	−7.05	−2.84	1.71	−11.25	−6.86	−1.26	1.34
$\mathrm{PAO_{theor}}$	−12.99	0.66	−10.56	−7.10	−2.88	1.88	−11.30	−6.92	−1.27	1.39
LAPW (Ref. 37)	−12.80	0.29	−10.29	−6.89	−2.69	1.35	−11.03	−6.70	−1.15	0.85
PW-PP (Ref. 38)	−12.56	0.55	−10.25	−6.70	−2.58	1.43	−10.95	−6.52	−1.09	1.02
LDA-PAO (Ref. 39)	−12.38	1.03	−9.85	−6.72	−2.66	1.59	−10.63	−6.53	−1.14	1.28
EXP (Ref. 40)	−13.10	1.63	−10.75	−6.70	−2.80	2.18	−11.24	−6.70	−1.30	1.85

crepancy found for Δ_{FA}. As we have just shown, such a deviation from the plane-wave calculation cannot be lifted by increasing the size of the basis, since this does not produce variations larger than 2%. A possible origin of such a disagreement may be the slightly different pseudopotentials used.

In Fig. 3 we present the magnetization as a function of the lattice constant for MnAs, and compare it with that obtained previously in our plane-wave calculations.[32] The agreement is quite good; the transition to the half-metallic state is correctly predicted for $a_0 = 5.8$ Å, and the dependence of the magnetization on the lattice spacing is well reproduced for $a_0 > 5.3$ Å. For smaller lattice spacings the two calculations disagree, with a tendency of the PAO basis to overstabilize the ferromagnetic phase. However, this is not surprising, since the portability of the pseudopotentials used in the two cases is different.

Finally we check the ability of our optimized basis set to describe the electronic and structural properties of GaAs, which forms the matrix where the Mn ions are included in $Ga_{1-x}Mn_xAs$. We find an equilibrium lattice constant of $a_0 = 5.635$ Å which is remarkably close to the experimental one. Moreover the bandstructure is very accurate; a comparison of our calculated eigenvalues with existing calculations is presented in Table II.

In summary, we are confident that the results, which we obtain using the numerical atomic orbital method with the combination of Troullier-Martins pseudopotentials and the basis set described in this section, are in good agreement with LSDA results obtained using other techniques.

III. ELECTRONIC CONFIGURATION OF GaAs:Mn

In this section we study the electronic structure of Mn in GaAs. We consider large GaAs cells (from two to 96 atoms) in which we replace one Ga atom with a Mn atom (Mn_{Ga}). We use 18 *k* points in the corresponding irreducible Brillouin zones for all the supercells, and over 1000 *k* points for the primitive zinc-blende unit cell (two atoms). Since the cell contains only one Mn atom and we use periodic boundary conditions, the Mn atoms are forced to be ferromagnetically aligned. For the smaller cells (32 and 48 atoms) we perform several simulations changing the shape of the unit cell. This is equivalent to investigating different arrangements of the Mn atoms with respect to each other. We find that, although the general properties do not change, different Mn ion arrangements in the cell result in different total energies. For all the calculations we assume the GaAs experimental lattice spacing $a_0 = 5.65$ Å.

A. Partial DOS and charge-density distribution

We start by analyzing the orbital-resolved density of states. In Fig. 4 we present as an example the DOS obtained for a 64-atom unit cell with one Mn_{Ga} substitution. Similar features are obtained for both higher and lower Mn concentrations. Far from the Fermi energy the DOS remains close to the DOS of GaAs (see Fig. 4), with a lower-energy As-*s* band and a Ga(*s*)-As(*p*) valence band. At the Fermi energy the situation is markedly different. The majority-spin band has a rather sharp peak, characteristic of a narrow band, while the minority-spin has a gap. Such a band structure is the signature of a half-metallic material. The total magnetization of the cell is $4\mu_B$. Our calculations for higher and lower Mn concentrations show that the magnetization does not change with the Mn concentration. In the minority band the corresponding peak is shifted to higher energy, and is very close to the edge of the GaAs conduction band. If we now consider the DOS projected onto the different orbital components of the wave function, and look at the *e* and t_2 *d* states of Mn, some interesting features appear. The majority band exhibits two broad peaks between -4 and -1 eV below the Fermi energy, with strong *e* and t_2 components, respectively. In addition there is a rather narrow t_2 peak at the Fermi energy. In contrast the minority band has almost no *d* character below E_F but instead has two sharp *e* and t_2 peaks around 1 eV above E_F. The different peak widths reflect the different degrees of hybridization of the Mn-*d* band with the GaAs bands. The hybridization is much stronger for states far below the Fermi energy.

In order to have a better understanding of the *p-d* hybridization in diluted $Ga_{1-x}Mn_xAs$, in Fig. 5 we present the evolution of the Mn-*d* peaks as a function of the Mn concentration. The most relevant feature is that for the sharp peaks in both the majority and minority bands [columns (b) and (c)] the *relative* intensity of the *d* component of the DOS is independent of the Mn concentration. Therefore, those portions of the DOS must be derived almost entirely from the Mn impurity and its four neighboring As atoms. This can also be seen by looking at the DOS projected onto the *p* states of the four atoms tetrahedrally coordinated with Mn (the dot-dashed line of Fig. 5). In summary, our analysis

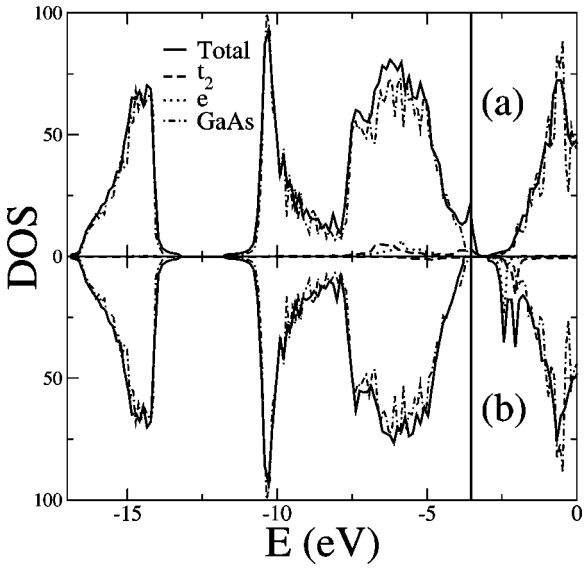

FIG. 4. Partial density of state for $Ga_{1-x}Mn_xAs$ for $x = 0.3$ (one Mn_{Ga} in a 64-atom GaAs cell): (a) majority spin, (b) minority spin. The vertical line denotes the position of the Fermi energy. The dashed and dotted lines represent the projection of the DOS onto the Mn-*d* t_2 and *e* orbitals, respectively. The dot-dashed line represents the DOS for GaAs.

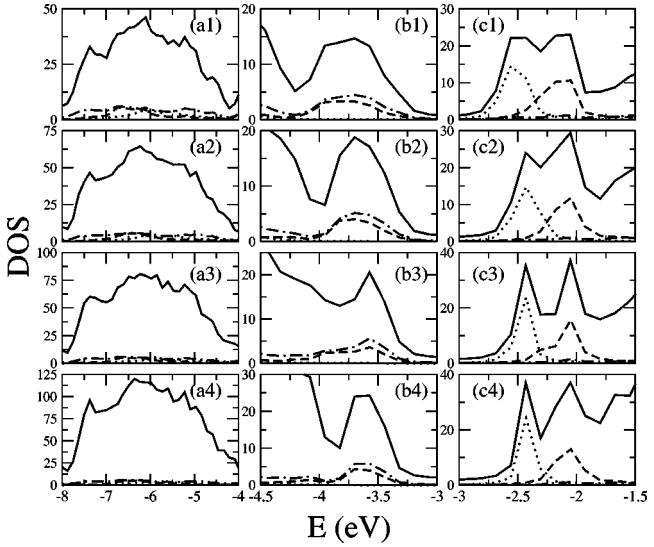

FIG. 5. Total and orbital-resolved DOS's for different Mn concentrations. The three columns correspond to different energy regions and spins: (a) majority band between -4 and -1 eV below E_F (broad Mn-d peaks), (b) majority band at the Fermi energy (sharp Mn-d peak), and (c) minority band 1 eV above E_F. The four rows indicate different Mn concentrations: (1) $x=0.06$ (one Mn in 32 atoms), (2) $x=0.04$ (one Mn in 48 atoms), (3) $x=0.03$ (one Mn in 64 atoms), and (4) $x=0.02$ (one Mn in 96 atoms). The solid lines denote the total DOS, while the dashed, dotted, and dot-dashed lines denote the DOS's coming from the t_2 states of Mn, the e states of Mn, and the As(p) states of the four As atoms neighboring the Mn impurity, respectively. Note that states of columns (b) and (c) do not scale with the concentration, indicating strong local hybridization.

shows that the $MnAs_4$ complex accounts for most of the DOS at the valence-band edge for the majority band and at the conduction-band edge for the minority band.

In contrast, the Mn-d states far below E_F result from strong coupling with the p orbitals of all the As atoms of the GaAs cell. This can be clearly seen in Fig. 6, where we present the charge-density isosurface plots corresponding to the three DOS's of Fig. 5. Figure 6 shows that the charge corresponding to states at the edge of the GaAs band gap is localized around the $MnAs_4$ complex [Figs. 6(b) and 6(c)], while the remaining Mn-d states are hybridized with all the As-p orbitals [Fig. 6(a)].

We now turn our attention to the distribution of the magnetization around the Mn ion. The magnetization around one atom placed at $\mathbf{R_0}$ is calculated as

$$M(R_i)=\int_{\Omega_{R_i}}[\rho_\uparrow(\mathbf{r}-\mathbf{R_0})-\rho_\downarrow(\mathbf{r}-\mathbf{R_0})]dr, \qquad (2)$$

where Ω_{R_i} is a sphere of radius R_i and ρ_σ is the charge density for the spin σ. The charge density is calculated on a real-space grid by evaluating the localized orbitals on such a grid.[24] Of course $M(R_i)$ depends on the cutoff radius R_i. In Fig. 7 we present the magnetization of Mn, and of the first and second As nearest neighbors of Mn as functions of R_i.

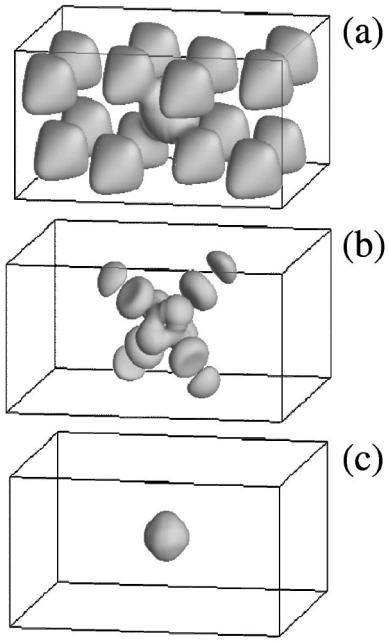

FIG. 6. Charge-density isosurfaces for the three states shown in Fig. 5. In this case we consider only $x=0.06$ (one Mn in a cubic 32-atom cell). (a) Majority band between -4 and -1 eV below E_F (broad Mn-d peaks). (b) Majority band at the Fermi energy (sharp Mn-d peak). (c) Minority band 1 eV above E_F. The Mn ion is in the center of the cell.

In the case of Mn the magnetization saturates for $R_i=4.0$ a.u., and remains almost constant up to $R_i\sim 18.0$ a.u. when the next Mn shell is encountered. Hence we can easily deduce that the Mn magnetization is $4\mu_B$, which is the saturation value. In contrast the magnetization around the As ions shows a negative minimum (between 2 and 3 a.u. from the As ion, depending on the position of the As ion relative to the Mn ion), followed by a sharp increase. The minimum corresponds to a negative spin polarization with respect to the Mn, and the following magnetization increase occurs at distances where the polarization of the neighboring atoms starts to be included in the integration. In the case of a first-nearest neighbor this magnetization increase is due mainly to the spin polarization of Mn [Fig. 7(b)] and in the case of second-nearest neighbors it is due to the four Ga ions coordinated to As [Fig. 7(c)]. It is interesting to note that the polarization of the As ion is always negative with respect to that of Mn. This means that Mn and As are antiferromagnetically coupled. The values of the spin polarizations of As at the minima are $-0.03\mu_B$ and $-0.005\mu_B$, respectively, for first- and second-nearest neighbors. These values of polarization are similar to those already published for GaAs/MnAs superlattices calculated with a first-principles linear-muffin-tin orbital–atomic-sphere-approximation method.[41] It is worth noting that we did not find any sizable changes in the magnetization per atom as a function of the Mn concentration for all the concentrations studied.

Finally we compare the orbital resolved DOS of $Ga_{1-x}Mn_xAs$ with that of zinc-blende structure MnAs. In Fig. 8 we present the DOS for zinc-blende MnAs with the lattice spacing of GaAs (5.65 Å), which is the same lattice

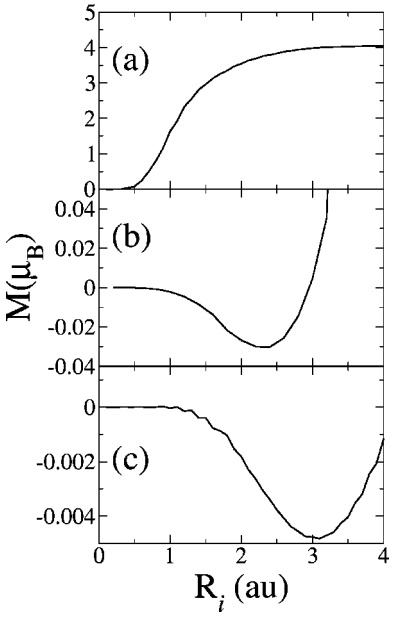

FIG. 7. Magnetization profile as a function of the integration radius R_i for $Ga_{1-x}Mn_xAs$ with $x=0.03$ (one Mn ion in a cubic 64-atom GaAs cell). (a) Mn. (b) First-nearest As atom to Mn. (c) Second-nearest As atom to Mn.

spacing that we used for diluted $Ga_{1-x}Mn_xAs$. For this lattice spacing MnAs is not a half-metal, since the Fermi energy in the minority band cuts through the conduction-band edge, mainly dominated by *d* electrons. Although the total DOS is different the projection onto the *d*-orbitals closely resembles that of diluted $Ga_{1-x}Mn_xAs$ (see Fig. 4). In particular there is a large occupation of the *d* orbitals in the majority band, while in the minority band only the bands of t_2 symmetry are occupied as a result of the hybridization

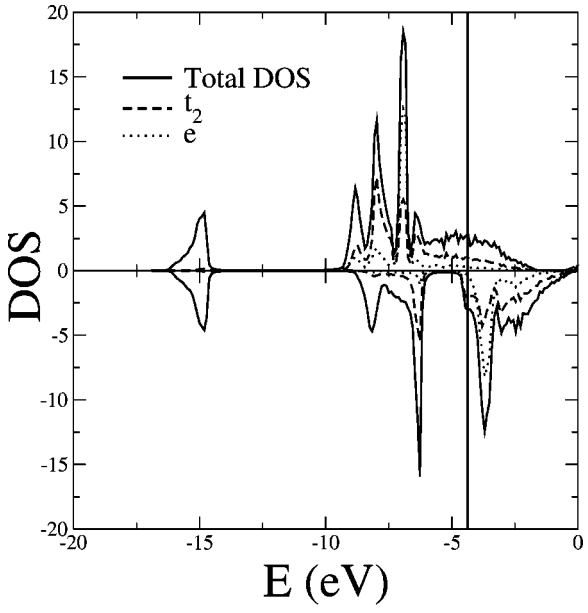

FIG. 8. Orbital-resolved DOS for zinc-blende MnAs with a lattice spacing of $a_0=5.65$ Å. The vertical line denotes the position of the Fermi energy.

with the As-*p* states at the edge of the valence band. The magnetization integrated around Mn ions is smaller in zinc-blende MnAs at this lattice constant than in $Ga_{1-x}Mn_xAs$. For a lattice spacing of $a_0=5.65$ Å we find a Mn polarization of $3.79\mu_B$, compared with $4.0\mu_B$ of $Ga_{1-x}Mn_xAs$. In contrast the polarization of As in zinc-blende MnAs is considerably larger, with an integrated magnetization of about $-0.17\mu_B$. We also note that on increasing the lattice spacing the spin polarization of Mn increases, but the polarization of the As is largely unchanged. For instance at $a_0=5.80$ Å we find $4.04\mu_B$ and $-0.17\mu_B$, respectively, for the Mn and As magnetizations. This suggests that the polarization of Mn is related to the ionicity of the bond with As.

A more quantitative comparison of the zinc-blende MnAs with diluted $Ga_{1-x}Mn_xAs$ can be obtained by performing Mülliken population analyses.[42,43] We describe the results of such analyses in Sec. III B.

B. Mülliken population analysis

We perform Mülliken population analyses[42,43] in order to compare quantitatively the orbital occupations of $Ga_{1-x}Mn_xAs$ at different dilutions. The Mülliken population analysis is a convenient way to separate different contributions to the total charge density. Suppose we have a system described by the wave-function $\phi=c_1\psi_1+c_2\psi_2$, where ψ_α is a localized function and c_α is the corresponding amplitude. Then, if the state ϕ is occupied by *N* electrons, the total occupation can be written as

$$N=Nc_1^2+2Nc_1c_2S_{12}+Nc_2^2, \tag{3}$$

where S_{12} is the overlap integral, $\int\psi_1\psi_2 dv$. Mülliken defined the subpopulations Nc_1^2 and Nc_2^2 as net populations, and $2Nc_1c_2S_{12}$ as overlap population. Moreover if the overlap population is equally split between the two wave functions, we obtain $Nc_1^2+Nc_1c_2S_{12}$ and $Nc_2^2+Nc_1c_2S_{12}$, respectively, which are referred to as gross populations. In what follows we always refer to the gross population. If the functions ψ_α represent orbital components of the angular momentum, then the populations correspond to orbital populations and the overlap population is the orbital overlap population. Similarly if the functions ψ_α are atomic wave functions for the atom α, then we obtain the atomic populations and the atomic overlap population. We also define Mülliken atomic charge as the difference between the gross atomic charge (i.e., $eNc_2^2+eNc_1c_2S_{12}$, with *e* the electronic charge) and the valence charge of the isolated atom. It is widely accepted that the absolute magnitude of the atomic charges can depend strongly on the basis set in which they are calculated.[44] However, relative values of Mülliken populations can provide useful information when comparing different systems (for instance, the amount of covalency in semiconductors).[45]

We start the analysis by calculating the Mülliken atomic charges for Ga, Mn, and As in GaAs, MnAs, and $Ga_{1-x}Mn_xAs$ at different concentrations (Table III). In the case of $Ga_{1-x}Mn_xAs$, for each atomic species we present the average values over the cell. Since we have already

TABLE III. Mülliken charges for GaAs, MnAs, and Ga_{1-x}, Mn_xAs at different Mn concentrations. The last two columns correspond, respectively, to the average over the As atom, excluding the ones coordinated with Mn, and the average over the four As atoms coordinated with Mn. The lattice spacing of MnAs is assumed to be $a_0 = 5.65$ Å.

Material	Ga ($\|e\|$)	Mn ($\|e\|$)	As ($\|e\|$)	As^{IV}($\|e\|$)
GaAs	+0.056		−0.056	
MnAs		−0.322	+0.332	
$Ga_{0.938}Mn_{0.062}As$	+0.042	−0.089	−0.046	+0.005
$Ga_{0.958}Mn_{0.042}As$	+0.046	−0.085	−0.049	+0.005
$Ga_{0.969}Mn_{0.031}As$	+0.047	−0.083	−0.049	+0.005
$Ga_{0.979}Mn_{0.021}As$	+0.049	−0.082	−0.050	+0.005

shown that the four As atoms coordinated with Mn (which we denote by As^{IV}) have quite different properties than the remaining As atoms, we calculate their average atomic charge separately. The table shows clearly the local character of the $MnAs_4$ center. We note that the average Mülliken charges of Ga and As closely resemble those of GaAs, particularly for low Mn concentrations. Of course in the extremely diluted limit GaAs:Mn one expects the average charges of Ga and As to be exactly those of GaAs. In contrast, the average Mülliken charge of the four As atoms coordinated with the Mn impurity does not change with the concentration, confirming that the electronic structure of the $MnAs_4$ complex is not affected by the concentration. It is also interesting to note that these As atoms have small positive atomic charges, whereas the other As atoms have negative atomic charges. A positive As atomic charge is also found in zinc-blende MnAs, although in that case its magnitude is much larger. The transition from GaAs:Mn to zinc-blende MnAs with increasing Mn concentration is reflected in the increase of Mülliken charge on the Mn atoms. Therefore, the Mn-As bond becomes more ionic when the Mn concentration is increased. This picture, together with the almost complete occupation of the *d* shells in the majority band discussed in Sec. III A, is consistent with modeling Mn in GaAs as an A^0 impurity center composed of a negatively charged Mn ion in a d^5 configuration, and a weakly bound hole (d^5+h).[46,47] The increase of the Mn concentration, and the consequent increase of the hole concentration, reduce the binding energy of the bound hole due to the partial screening of the potential. Therefore, an increase of the Mülliken charge of Mn with concentration is expected. Nevertheless the agreement is only qualitative, and a definitive prediction based solely on Mülliken analysis cannot be made.

We now turn our attention to the orbital population. In Table IV we present orbital populations for the *p* orbitals of As and *d* orbitals of Mn in MnAs and $Ga_{1-x}Mn_x$As for both spin orientations. As before, we distinguish between the As^{IV} atoms and the remaining As atoms. We do not report the orbital populations for Ga for the *s* orbital of As or for the *s* and *p* orbitals of Mn, since they are not relevant to the discussion.

Several important aspects can be pointed out from Table IV. The total population for the *d* orbital of Mn is around 5.5 electronic charges for all the systems studied. We do not expect integer values for the orbital population, since a strong *p-d* hybridization is present. The total overlap population for zinc-blende MnAs is about 0.6 electronic charges, and this can be considered to be the uncertainty on the determination of the orbital population. This gives Mn *d* orbital occupations of 4.6 ± 0.6 and 0.8 ± 0.6 for the majority and minority bands, respectively. Although the orbital population is not an observable quantity, and its absolute value may be affected by the choice of the basis set, we can conclude that the atomic configuration of Mn in GaAs is compatible with both $3d^5$ and $3d^6$. This is in agreement with recent x-ray-absorption magnetic circular dichroism experiments,[48] where the data are interpreted by assuming a Mn configuration consisting of 80% Mn $3d^5$ and 20% Mn $3d^6$. It is interesting to note that by decreasing the Mn concentration there is an increase of the polarization of the *d* orbital of Mn (the orbital population is enhanced in the majority band and reduced in the minority band). This seems to be in favor of the $A^- 3d^5$ configuration in the limit of high dilution, as reported extensively in the literature.[46,47,49–51]

Table IV also shows clearly that there is antiferromagnetic coupling between the Mn *d* and As *p* orbitals. The As *p* orbitals in fact have quite a large spin polarization as opposed to that of Mn. This cannot be due to the overlap components of the orbital population, which would give the same polarization as that of Mn. It is also interesting to note that the spin polarization is much larger among the As^{IV} atoms, for which it is almost insensitive to the Mn concentration, than among the other As atoms. As expected, it is still smaller than the As spin polarization in zinc-blende MnAs.

TABLE IV. Mülliken orbital populations in MnAs and Ga_{1-x}, Mn_xAs at different Mn concentrations. The symbols ↑ and ↓ correspond to majority and minority spins, respectively. The last two columns correspond to the four As atoms coordinated with Mn. The lattice spacing of MnAs is assumed to be $a_0 = 5.65$ Å.

Material	Mn-$d_\uparrow$($\|e\|$)	Mn-$d_\downarrow$($\|e\|$)	As-$p_\uparrow$($\|e\|$)	As-$p_\downarrow$($\|e\|$)	As^{IV}-$p_\uparrow$($\|e\|$)	As^{IV}-$p_\downarrow$($\|e\|$)
MnAs	4.642	0.855	1.365	1.650		
$Ga_{0.938}Mn_{0.062}As$	4.665	0.788	1.626	1.637	1.580	1.647
$Ga_{0.958}Mn_{0.042}As$	4.679	0.770	1.628	1.638	1.583	1.644
$Ga_{0.969}Mn_{0.031}As$	4.675	0.771	1.630	1.637	1.584	1.644
$Ga_{0.979}Mn_{0.021}As$	4.682	0.768	1.632	1.636	1.584	1.644

Nevertheless we also see that the other As atoms have a small antiferromagnetic polarization of the *p* orbital, which decreases with concentration as expected. This is in very good agreement with the magnetization data presented in Sec. III A.

IV. EXCHANGE COUPLING

As we pointed out in Sec. I, the evaluation of the exchange constant $N\beta$ is crucial for predicting the thermodynamic properties of $Ga_{1-x}Mn_xAs$. In this section we provide a theoretical estimate of the exchange constant, and study its dependence on the Mn concentration. We begin by briefly describing the effect of the *sp-d* exchange on the band structure of the host semiconductor in the mean-field approximation. Our starting point is the commonly used *sp-d* exchange Hamiltonian[20]

$$H_{sp\text{-}d}=-\frac{1}{2}\sum_i \sum_{n,k,k'} J_n^{sp\text{-}d}(\mathbf{k},\mathbf{k}')e^{i(\mathbf{k}-\mathbf{k}')\cdot\mathbf{R}_i}\mathbf{S}_i \times\left[\sum_{\mu\nu} c^{\dagger}_{n\mathbf{k}\mu}\sigma_{\mu\nu}c_{n\mathbf{k}'\nu}\right], \quad (4)$$

where $J_n^{sp\text{-}d}(\mathbf{k},\mathbf{k}')$ is the exchange integral of the band electrons $(n,\mathbf{k})$ and $(n,\mathbf{k}')$ with the Mn local spin $\mathbf{S}_i$, $c^{\dagger}_{n\mathbf{k}}$ and $c_{n\mathbf{k}}$ are the creation and annihilation operators for an electron in band n with Bloch vector $\mathbf{k}$. The sum extends over the valence $(n=v)$ and conduction $(n=c)$ bands of GaAs, and all the localized spins labeled by the index *i*. If we neglect interband terms which are negligible and replace the spin $\mathbf{S}_i$ by the average spin $\langle S\rangle$ proportional to the magnetization, we restore the translational invariance of the system. Therefore, expression (4) becomes diagonal in $\mathbf{k}$, and can be written as a function of the Mn fraction x and the cation concentration N as

$$H_{sp\text{-}d}=-\tfrac{1}{2}xN\langle S\rangle\sum_k J_n^{sp\text{-}d}(k)(c^{\dagger}_{nk\uparrow}c_{nk\uparrow}-c^{\dagger}_{nk\downarrow}c_{nk\downarrow}), \quad (5)$$

with $\uparrow$ ($\downarrow$) indicating the up-spin (down-spin) direction with respect to the mean-field spin $\langle S\rangle$ and $J_n^{sp\text{-}d}(k)=J_n^{sp\text{-}d}(\mathbf{k},\mathbf{k})$. If we now restrict our analysis to the band edge (Γ point), and define $\alpha=J_c^{sp\text{-}d}(0)$ and $\beta=J_v^{sp\text{-}d}(0)$, we obtain the equations

$$\begin{aligned} H_{sp\text{-}d}&=-\frac{1}{2}xN\langle S\rangle\alpha(c^{\dagger}_{c0\uparrow}c_{c0\uparrow}-c^{\dagger}_{c0\downarrow}c_{c0\downarrow}),\\ H_{sp\text{-}d}&=-\frac{1}{2}xN\langle S\rangle\beta(c^{\dagger}_{v0\uparrow}c_{v0\uparrow}-c^{\dagger}_{v0\downarrow}c_{v0\downarrow}), \end{aligned} \quad (6)$$

for the conduction and valence bands, respectively. We note that the same analysis can be carried out by assuming that the Mn impurities form a perfect ferromagnetic crystal. In such a case the derivation of Eqs. (6) is identical to that given here if the magnetic moment per Mn atom is used for the mean field spin $\langle S\rangle$. Equations (6) relate the spin splitting of the conduction and valence bands to the exchange integral calculated at $k=0$. This quantity is usually extracted in optical magnetoabsorption experiments from a spin splitting of the exciton lines. For instance the Zeeman splitting of the heavy-hole exciton transition E_1 is

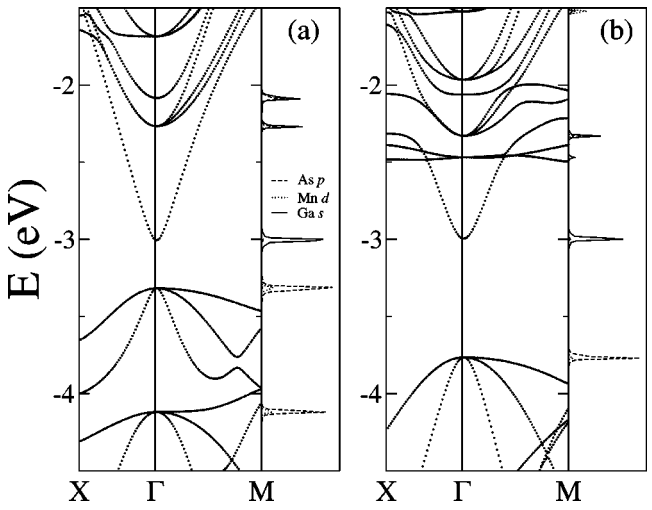

FIG. 9. Band structure and orbital-resolved DOS at the Γ point for $Ga_{1-x}Mn_xAs$, with $x=0.3$ (one Mn ion in a cubic 64-atom GaAs cell): (a) majority band, (b) minority band.

$$E_1=x\langle S\rangle N(\beta-\alpha). \quad (7)$$

Other transitions give different combinations of α and β, which can then be determined. Note, finally, that the spin splitting of both the valence and conduction bands in the mean-field approximation is linear with the Mn concentration x.

We calculate the exchange constants directly from the conduction-band-edge (valence-band-edge) spin-splittings $\Delta E^c=E^c_{\downarrow}-E^c_{\uparrow}$ $(\Delta E^v=E^v_{\downarrow}-E^v_{\uparrow})$ as

$$N\alpha=\Delta E^c/x\langle S\rangle, \quad N\beta=\Delta E^v/x\langle S\rangle, \quad (8)$$

where $\langle S\rangle$ is half of the computed magnetization per Mn ion. In order to evaluate the parameters in Eqs. (8), we compute the band structure around the Γ point for large GaAs cells with a single Mn impurity. In Fig. 9 we present, as an example, the results for a cubic cell containing 64 atoms. Since we are mainly interested in the Γ point, we consider the band structure only along the direction $[1/8(\pi/c_0),0,0]\rightarrow(0,0,0)\rightarrow[1/8(\pi/c_0),1/8(\pi/c_0),1/8(\pi/c_0)]$, with c_0 the unit vector of the cubic cell. We indicate these two directions respectively as *X* and *M*. In Fig. 9 we also plot the orbital-resolved DOS at the Γ point. This shows clearly that the valence-band edge has mainly As-*p* character, with additional contributions from t_2 Mn-*d* states due to hybridization, while the conduction-band edge is formed by Ga-*s* states. In this way the spin splitting is easily computed.

We consider different Mn concentrations and, for smaller unit cells (larger concentrations), different geometrical arrangements. We find that the spin splittings of both the conduction and valence bands are dependent on the relative positions between the Mn ions, with variations of up to 20%. In particular for the same Mn concentration we find large splittings when the Mn ions are clustered, and smaller splittings

TABLE V. Conduction ΔE^c and valence ΔE^v band-edge spin splittings, and exchange constants as a function of the Mn concentration x for $Ga_{1-x}Mn_xAs$.

x	ΔE^c (eV)	ΔE^v (eV)	$N\alpha$ (eV)	$N\beta$ (eV)
0.062 50	0.0339	−0.6839	0.272	−5.48
0.041 66	0.0248	−0.5458	0.298	−6.54
0.031 25	0.0105	−0.4472	0.168	−7.34
0.020 84	0.0099	−0.3442	0.234	−8.16

for homogeneously diluted systems. More details on the dependence of the exchange constant on the spatial arrangement of the Mn ions will be published elsewhere.[52] In the following we consider only cells which maximize the separation between the Mn ions (uniform Mn distribution).

In Table V we present the spin splittings for the conduction and valence bands as functions of the Mn concentration, and we list the corresponding exchange constants. First consider the conduction band. Although the spin splitting shows large fluctuations with x, there is no systematic variation with the Mn concentration. With the caveat that DFT is a ground-state theory and therefore does not accurately describe the conduction band, from Table V one can conclude that the coupling (s-d coupling) between the conduction band of GaAs and the Mn impurity is ferromagnetic. Also, it is independent of x, as predicted by mean-field theory, and has the value $N\alpha \sim 0.2$ eV. Note that ferromagnetic coupling is expected, since in the case of the conduction band the only exchange is direct; in addition, the value of the exchange constant $N\alpha$ is very close to that usually found in II-VI semiconductors.[53]

The situation is quite different for the valence band. First of all, we see that the spin splitting of the valence-band edge is much larger than the typical absorption edge splitting in magnetoptical experiments.[16] For instance, if we compare the results for $x=0.032$ of Ref. 16 with those of Table V for the same concentration, we find that our calculated value is about four times larger than that obtained experimentally. However, it is important to point out that in our calculation all the Mn ions contribute to the ferromagnetism. In contrast, in real systems only a fraction of the Mn ions are ferromagnetically aligned, and the typical magnetization curves have a large paramagnetic component which does not saturate even at very high magnetic fields.[54] This was confirmed by recent x-ray magnetic dichroism measurements.[48] Assuming a mean-field picture, this suggests that the mean-field spin calculated here is much larger than that present in actual samples. Turning the argument around, we can conclude that our results are consistent with experiments if we assume that in the latter the effective Mn concentration (contributing to the ferromagnetism) is only one-fourth of the nominal concentration.

A second important point is that the exchange constant $N\beta$ is strongly dependent on x. Specifically, $N\beta$ increases with decreasing Mn concentration, a behavior already well known to occur in $Co_{1-x}Mn_xS$.[55–57] This dependence of the exchange constant on x could be due to two possible reasons: (i) the actual p-d coupling is not Kondo-like, or (ii) the mean-field approximation that leads to Eq. (5) is not valid. Blinowski and Kacman studied the kinetic exchange interaction of various $3d$ metal impurities in zinc-blende semiconductors.[58] By applying canonical transformations to the p-d hybridization Hamiltonian,[59] they evaluated the effective exchange interaction between the valence band and the d states of the impurity. They found that for $3d^5$ and $3d^6$ configurations of the impurity the effective exchange has a Kondo-like form, while there are other non-Kondo-like contributions for the $3d^4$ case. From Mülliken analysis we can rule out this latter configuration, and conclude that the effective exchange is indeed Kondo-like. Therefore, the dependence of $N\beta$ on x is suggestive of the breakdown of the mean-field approximation.

V. BREAKDOWN OF MEAN-FIELD APPROXIMATION

The main hypothesis sustaining the mean-field approximation is that the potential introduced by the Mn ions is weak with respect to the relevant bandwidth. This seems to be true in most of the II-VI semiconductors; however, in the case of (Cd, Mn)S such a hypothesis breaks down, and an apparent strong dependence of the exchange constant on the Mn concentration is found.[55–57] The case of Mn in GaAs looks very similar. We recall that for the very diluted limit there is some evidence of the Mn ion being able to bind a polarized hole.[51] This suggests that the potential created by Mn in GaAs may be strong, and hence the mean-field approximation breaks down.

Benoit à la Guillaume, Scalbert, and Dietl[60] calculated the corrections to the mean-field approximation using a free-electron model, with the magnetic impurities described by square potentials. The energy was calculated within the Wigner-Seitz approach, which is applicable only to the case of perfectly periodic crystal. Although the model was refined,[61,62] the main findings are still valid. Here we illustrate briefly the model and we use it for computing the exchange constant.

We consider a free-electron model with effective mass m^*, and uniformly distributed magnetic impurities described by the potential

$$U(r)=W(r)-J(r)\mathbf{S}\cdot\mathbf{s}. \tag{9}$$

Here $W(r)$ is the spin-independent substitutional potential, and $J(r)$ is the p-d coupling between the free-electron spin $\mathbf{s}$ and the impurity spin $\mathbf{S}$. We further assume that $J(r)$ and $W(r)$ have the same square potential shape, and that all the impurity spins are ferromagnetically aligned. This leads to $U(r)=U_0\theta(r-b)$, and also $U^{\uparrow(\downarrow)}(r)=(W\mp 5/4J)\,\theta(r-b)$, when $S=\frac{5}{2}$ is considered. Finally the energy is calculated by solving a transcendental equation obtained by imposing the appropriate boundary conditions.[60] We define $\delta(x,U_0)=E(x,U_0)/E_{\mathrm{mfa}}(x,U_0)$ as the deviation of the computed energy $E(x,U_0)$ from the mean field energy $E_{\mathrm{mfa}}(x,U_0)=VNx$, where $V=(4\pi/3)b^3U_0$, and Nx is the Mn density. In Fig. 10 we present $\delta(x)$ as a function of x for different potentials $\eta=U_0/|U_c|$, where $U_c=-(\pi\hbar/2b)^2/2m^*$ is the binding potential. We note that the corrections to mean-field theory are large for small x, and decrease with increasing x.

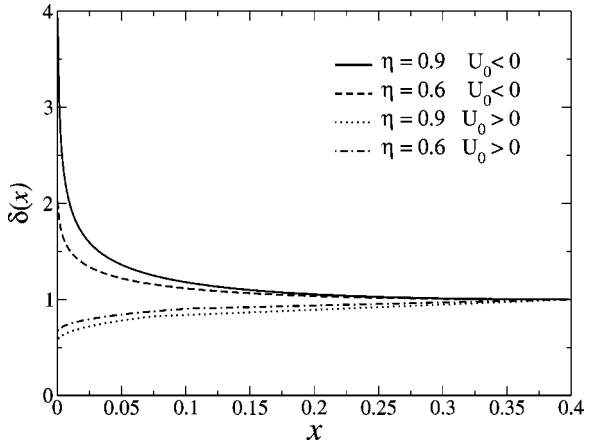

FIG. 10. Dependence of the correction factor $\delta(x)$ on the impurity concentration x for a range of potentials. Note that the deviation from mean-field theory is larger for strongly attractive potentials.

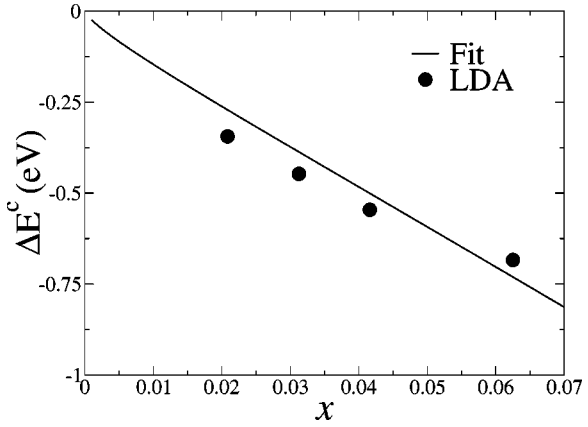

FIG. 11. Band-edge spin splitting: the circles represent our LDA data, and the straight line the fit obtained with the model discussed in the text for the parameters $b=3.6$ Å, $J=-1.05$ eV ($N\beta=-4.5$ eV), and $W=-0.027$ eV.

In particular the mean-field approximation breaks down when the potential is attractive and close to the binding potential ($\eta\rightarrow 1$), while it is reasonably good for repulsive potentials. We also note that the mean-field approximation is recovered in both the limit of large Mn concentrations ($x\rightarrow 1$) and in the limit of weak potential ($\eta\rightarrow 0$). This general behavior can qualitatively explain our LDA results. Consider, in fact, the band-edge spin splitting

$$\Delta E^c(x)=\frac{4\pi b^3}{3}[(W+5/4J)\,\delta(x,\eta^{\downarrow}) - (W-5/4J)\,\delta(x,\eta^{\uparrow})]Nx, \qquad (10)$$

where $\eta^{\uparrow(\downarrow)}=(W\mp 5/4J)/|U_c|$. By comparing Eq. (10) with Fig. 10, one can see that for small x the spin splitting is largely enhanced with respect to its mean-field value. The deviation diminishes with increasing x, and vanishes in the limit of complete Mn substitution ($x=1$). Note that the application of the mean-field approximation at every x gives rise to an apparent increase of the exchange constant with the Mn concentration. This agrees with our LDA results.

It is also worth noting that the deviation from mean-field theory is larger if the spin asymmetry of the potential U_0 is large. In particular, the spin splitting is largest when the potential is attractive for one spin species and repulsive for the other. In the opposite limit, when the mean-field approximation is valid ($\delta\rightarrow 1$), Eq. (10) reduces to the usual expression

$$\Delta E^c(x)=\tfrac{5}{2}N\beta x, \qquad (11)$$

where we have defined the exchange constant $N\beta=N(4\pi b^3/3)J$.

In order to compare with experiments, we perform a fit of our LDA data. We consider b, W, and J as fitting parameters, with b varying between the cation-anion and cation-cation distances, and W and J chosen so that no bound holes are present. This last restriction takes into account the lack of any experimental evidence for bound holes at the concentrations investigated here. The fitting procedure yields $b=3.6$ Å and $N\beta=-4.5$ eV, although values in the range $3.6\text{ Å}<b<3.9\text{ Å}$ and $-4.9\text{ eV}<N\beta<-4.4$ eV fit equally well. It is important to note that, for all the parameter sets which give a good fit, one spin hole is nearly bound while the other ''feels'' a weak repulsive potential. Our best fit is presented in Fig. 11. Despite the roughness of the model the agreement is reasonably good. It is interesting to point out that the model seems to underestimate the spin splitting for small x and overestimate it for large x. This is not surprising; in this model we assume that the potential induced by the magnetic impurity does not depend on the impurity concentration. This is in general true for Mn in II-VI semiconductors, where Mn provides only a local spin. In the case of III-V semiconductors, however, Mn acts both as an acceptor and as a source of localized spins. Therefore it is natural to expect a progressive screening of the Mn potential with concentration due to the increase of the hole density. This effect, which is responsible for the lack of bound holes in low diluted (Ga, Mn)As, further reduces the deviation from the mean-field approximation for large x, and better agreement with our LDA data may be found.

Finally we want to point out that the exchange constant found with the above analysis is still rather large compared with experiments. Although in actual samples part of the Mn ions does not contribute to the ferromagnetism, leading to an underestimate of $N\beta$, this probably cannot completely account for the discrepancy with our calculated value. It is well known that the local-density approximation is not very accurate in describing strongly localized charges as in Mn-d shells. In nonmagnetic semiconductors,[63] this leads to an overestimation of the p-d coupling and to an overbinding of the system. We found the same kind of behavior in NiAs-type MnAs (Ref. 32), with a volume compression of about 8%. This suggests that in our calculations the p-d coupling may be overestimated. However, since the volume compression of MnAs is not very large, we think that the error in the determination of the p-d coupling is not dramatic. Therefore our main conclusion, that the mean-field approximation breaks down for $Ga_{1-x}Mn_xAs$, is still valid.

VI. CONCLUSIONS

We have theoretically investigated the magnetic properties of $Ga_{1-x}Mn_xAs$ with dilutions ranging from $x=1$ to 0.02. We found that Mn in GaAs has an atomic configuration compatible with both $3d^5$ and $3d^6$, and that the total occupation is not integer because of the strong *p-d* coupling with the valence band of GaAs. Such a coupling is antiferromagnetic, with a remarkably large exchange constant. We have shown that the exchange constant has an apparent dependence on the Mn concentration. This suggests that the generally used mean-field approximation breaks down, since the potential induced by the Mn ions in GaAs cannot be treated perturbatively. Using a simple free-electron model, we have calculated corrections to the mean-field expression for the spin splitting of the GaAs valence band, and found a good agreement with the LDA calculations. Further study is needed to determine the dependence of the spin splitting on the confinement of the Mn ions in the case of highly ordered alloys.

ACKNOWLEDGMENTS

This work made use of MRL Central Facilities supported by the National Science Foundation under award No. DMR96-32716. This work was supported by the DARPA/ONR under Grant No. N0014-99-1-1096, by ONR Grant No. N00014-00-10557, by NSF-DMR under Grant No. 9973076, and by ACS PRF under Grant No. 33851-G5. P.O. acknowledges support from Fundación Ramón Areces (Spain). Useful discussions with N. Samarth, D. D. Awschalom, and L. J. Sham are kindly acknowledged.

*Electronic address: ssanvito@mrl.ucsb.edu

[1] H. Ohno, H. Munekata, T. Penney, S. von Molnar, and L. L. Chang, Phys. Rev. Lett. **68**, 2664 (1992).
[2] H. Ohno, A. Shen, F. Matsukura, A. Oiwa, A. Endo, and S. Kutsumoto, Appl. Phys. Lett. **69**, 363 (1996).
[3] H. Ohno, J. Magn. Magn. Mater. **200**, 110 (1999).
[4] H. Ohno, Science **281**, 951 (1998).
[5] G. Prinz, Phys. Today **48(4)**, 58 (1995).
[6] J. M. Kikkawa and D. D. Awschalom, Phys. Rev. Lett. **80**, 4113 (1998).
[7] J. M. Kikkawa and D. D. Awschalom, Nature (London) **397**, 139 (1998).
[8] Y. Ohno, D. K. Young, B. Beschoten, F. Matsukura, H. Ohno, and D. D. Awschalom, Nature (London) **402**, 790 (1999).
[9] G. Schmidt, D. Ferrand, L. W. Molenkamp, A. T. Filip, and B. J. van Wees, Phys. Rev. B **62**, R4790 (2000).
[10] D. P. Di Vincenzo, Science **270**, 255 (1995).
[11] T. Dietl, H. Ohno, F. Matsukura, J. Cibèrt, and D. Ferrand, Science **287**, 1019 (2000).
[12] T. Dietl, H. Ohno, and F. Matsukura, preprint cond-mat/0007190.
[13] H. Akai, Phys. Rev. Lett. **81**, 3002 (1998).
[14] J. Szczytko, W. Mac, A. Stachow, A. Twardowski, P. Becla, and J. Tworzydlo, Solid State Commun. **99**, 927 (1996).
[15] K. Ando, T. Hayashi, M. Tanaka, and A. Twardowksi, J. Appl. Phys. **83**, 6548 (1998).
[16] J. Szczytko, W. Mac, A. Twardowski, F. Matsukura, and H. Ohno, Phys. Rev. B **59**, 12 935 (1999).
[17] F. Matsukura, H. Ohno, A. Shen, and Y. Sugawara, Phys. Rev. B **57**, R2037 (1998).
[18] T. Omiya, F. Matsukura, T. Dietl, Y. Ohno, T. Sakon, M. Motokawa, and H. Ohno, Physica E (Amsterdam) **7**, 976 (2000).
[19] J. Okabayashi, A. Kimura, O. Rader, T. Mizokawa, A. Fujimori, T. Hayashi, and M. Tanaka, Phys. Rev. B **58**, R4211 (1998).
[20] B. E. Larson, K. C. Hass, H. Ehrenreich, and A. E. Carlsson, Phys. Rev. B **37**, 4137 (1988).
[21] J. Szczytko, W. Mac, A. Stachow, A. Twardowski, P. Becla, and J. Tworzydlo, Solid State Commun. **99**, 927 (1996).
[22] H. Hohenberg and W. Kohn, Phys. Rev. B **136**, B864 (1964); W. Kohn and L. Sham, Phys. Rev. A **140**, A1133 (1965).
[23] P. Ordejón, D. Sánchez-Portal, E. Artacho, and J. M. Soler, SIESTA, Spanish Initiative for Electronic Simulations with Thousands of Atoms.
[24] D. Sánchez-Portal, P. Ordejón, E. Artacho, and J. M. Soler, Int. J. Quantum Chem. **65**, 453 (1997), and references therein.
[25] P. Ordejón, Phys. Status Solidi B **217**, 335 (2000).
[26] D. M. Ceperley and B. J. Alder, Phys. Rev. Lett. **45**, 566 (1980).
[27] P. Pulay, Chem. Phys. Lett. **73**, 393 (1980).
[28] N. Troullier and J. L. Martins, Phys. Rev. B **43**, 1993 (1991).
[29] S. G. Louie, S. Froyen, and M. L. Cohen, Phys. Rev. B **26**, 1738 (1982).
[30] L. Kleinman and D. M. Bylander, Phys. Rev. Lett. **48**, 1425 (1982).
[31] G. Theurich (private communication). The calculations were performed with the code SPINOR which is a general-spin implementation of density-functional theory including spin-orbit interaction written in C. The code is publically available at http://www.mrl.ucsb.edu/~theurich/Spinor/
[32] S. Sanvito and N. A. Hill, Phys. Rev. B **62**, 15 553 (2000).
[33] E. Artacho, D. Sanchez-Portal, P. Ordejón, A. García, and J. M. Soler, Phys. Status Solidi **215**, 809 (1999).
[34] O. F. Sankey and D. J. Niklewski, Phys. Rev. B **40**, 3979 (1989).
[35] J. Izquierdo, A. Vega, L. C. Balbás, D. Sánchez-Portal, J. Junquera, E. Artacho, J. M. Soler, and P. Ordejón, Phys. Rev. B **61**, 13 639 (2000).
[36] M. Calleja, C. Rey, M. M. G. Alemany, L. J. Gallego, P. Ordejòn, D. Sánchez-Portal, E. Artacho, and J. M. Soler, Phys. Rev. B **60**, 2020 (1999).
[37] C. Filippi, D. J. Singh, and C. J. Umirigar, Phys. Rev. B **50**, 14 947 (1994).
[38] V. Fiorentini, Phys. Rev. B **46**, 2086 (1992).
[39] R. W. Jansen and O. F. Sankey, Phys. Rev. B **36**, 6520 (1987).
[40] *Semiconductors, Physics of Group IV Elements and III-V Compounds*, edited by O. Madelung, Landolt-Börnstein, New Series, Group III, Vol. 17, Pt. a (Springer-Verlag, Berlin, 1991).
[41] T. Ogawa, M. Shirai, N. Suzuki, and I. Kitagawa, J. Magn. Magn. Mater. **196-197**, 428 (1999).
[42] R. S. Mülliken, J. Chem. Phys. **23**, 1833 (1955).
[43] R. S. Mülliken, J. Chem. Phys. **23**, 1841 (1955).
[44] E. R. Davidson and S. Chakravorty, Theor. Chim. Acta **83**, 319 (1992).
[45] M. D. Segall, R. Shah, C. J. Pickard, and M. C. Payne, Phys. Rev. B **54**, 16 317 (1996).
[46] J. Schneider, U. Kaufmann, W. Wilkening, M. Baeumler, and F.

Köhl, Phys. Rev. Lett. **59**, 240 (1987).
[47] A. Twardowski, Mater. Sci. Eng., B **63**, 96 (1999).
[48] H. Ohldag, V. Solinus, F. U. Hillebrecht, J. B. Goedkoop, M. Finazzi, F. Matsukura, and H. Ohno, Appl. Phys. Lett. **76**, 2928 (2000).
[49] A. K. Bhattacharjee and C. Benoit à la Guillaume, Solid State Commun. **113**, 17 (2000).
[50] V. F. Sapega, T. Ruf, and M. Cardona, Solid State Commun. **114**, 573 (2000).
[51] M. Linnarsson, E. Janzén, B. Monemar, M. Kleverman, and A. Thilderkvist, Phys. Rev. B **55**, 6938 (1997).
[52] S. Sanvito and N. A. Hill, cond-mat/0011372 (unpublished).
[53] *Diluted Magnetic Semiconductors*, edited by J. K. Furdyna and J. Kossut, Semiconductor and Semimetals Vol. 25 (Academic, New York, 1988); *Diluted Magnetic Semiconductors*, edited by M. Balkanski and M. Averous (Plenum, New York, 1991).
[54] A. Oiwa, S. Kutumoto, A. Endo, M. Hirasawa, Y. Iye, H. Ohno, F. Matsukura, A. Shen, and Y. Sugawara, Solid State Commun. **103**, 209 (1997).
[55] V. G. Abrammishvili, S. I. Gubarev, A. V. Komarov, and S. M. Ryabchenko, Fiz. Tverd. Tela (Leningrad) **26**, 1095 (1984) [Sov. Phys. Solid State **26**, 666 (1984)].
[56] S. I. Gubarev and M. G. Tyazhlov, Fiz. Tverd. Tela (Leningrad) **32**, 635 (1990) [Sov. Phys. Solid State **32**, 373 (1990)].
[57] S. I. Gubarev and M. G. Tyazhlov, Pis'ma Zh. Eksp. Teor. Fiz. **44**, 385 (1986) [JETP Lett. **44**, 494 (1986)].
[58] J. Blinowski and P. Kacman, Phys. Rev. B **46**, 12 298 (1992).
[59] R. H. Parmenter, Phys. Rev. B **8**, 1273 (1973).
[60] C. Benoit à la Guillaume, D. Scalbert, and T. Dietl, Phys. Rev. B **46**, 9853 (1992).
[61] D. Scalbert, A. Ghazali, and C. Benoit à la Guillaume, Phys. Rev. B **48**, 17 752 (1993).
[62] J. Tworzydlo, Phys. Rev. B **50**, 14 591 (1994).
[63] S. B. Zhang, S.-H. Wei, and A. Zunger, Phys. Rev. B **52**, 13 975 (1995).